7-1-2006

Numerical Simulation and Graphical Analysis of In Vitro Benign Tumor Growth: Application of Single-Particle State Bosonic Matter Equation with Length Scaling

Pradip K. Biswas
Cleveland State University, pbiswas@tougaloo.edu

Jiansen Niu
Cleveland State University

Tobias Frederico
Instituto Tecnológica de Aeronáutica

Valentin Gogonea
Cleveland State University, V.GOGONEA@csuohio.edu

Publisher's Statement

The final publication is available at Springer via http://dx.doi.org/10.1007%2Fs00894-005-0095-6

Pradip K. Biswas · Jiansen Niu
Tobias Frederico · Valentin Gogonea

Numerical simulation and graphical analysis of in vitro benign tumor growth: application of single-particle state bosonic matter equation with length scaling

Abstract We describe the application of a non-linear single-particle state bosonic condensate equation to simulate multicellular tumor growth by treating it as a coupling of two classical wave equations with real components. With one component representing the amplitude of the cells in their volume growth phase and the other representing the amplitude of the cells in their proliferation or mitosis phase, the two components of the coupled equation feed each other during the time evolution and are coupled together through diffusion and other linear and non-linear terms. The features of quiescent and necrotic cells, which result from poor nutrient diffusion into a tumor, have been found to correspond quite well to experimental data when they are modeled as depending on higher cell density. Classical hallmarks of benign tumor growth, such as the initial rapid growth, followed by a dramatic collapse in the proliferating cell count and a strong re-growth thereafter appear quite encouragingly in the theoretical results. A tool for graphical analysis of the tumor simulation results has been developed to provide morphological information about tumors at various growth stages. The model and the graphical analysis can be extended further to create an effective tool to predict/monitor tumor growth.

Keywords Multicellular tumor · Computer simulation · Heisenberg equation · Length scaling

Introduction

Tumors arise as a consequence of unrestricted cell division. This unrestricted cell division is supposed to be possible due to a mutation of the *p53* transcription factor, which otherwise functions as a tumor suppressor gene in normal tissues. In response to DNA damage, *p53* activation results either in the induction of the cyclin-dependent kinase inhibitor *p21* and cell cycle arrest or in the induction of genes that induce programmed cell death through the transcriptional factor *p53*. One molecular mechanism through which unrestricted cell growth can be achieved is through mutation of *p53*. Mutated non-functional *p53* can no longer induce either cell cycle arrest or programmed cell death in response to DNA damage [1].

Thus, we can associate the functional role of the *p53* protein in cells (the biological building blocks) with that of the Pauli exclusion principle, which restricts the fermions (the elementary building blocks of matter) in occupying the same quantum state. On the other hand, bosons do not obey the Pauli exclusion principle, and a single-particle bosonic state can be occupied by any number of bosons. Thus, the statistical behavior of fermions and bosons resembles that of normal and cancer cells, where the number of normal cells is regulated by *p53* protein while the population of cancer cells is unregulated. In the same way as fermions and bosons are distinguished by their spins (half-integral for fermions and integral for bosons), normal and cancer cells may be distinguished by the presence of a wild type or mutated *p53* gene.

Guided by this analogy, a mathematical equation relating to a single-particle bosonic state was applied to the growing cancer cells in a tumor state with relative length-scaling [2, 3].

The primary impetus in applying such a model to tumor growth was that the growth dynamics of a single-particle state bosonic condensate matter and that of a multicellular tumor of cancer cells may follow the same mathematical equation but with different length scales. Such modeling may provide us crucial information about tumor morphology and be applied in simulations of tumor-drug interactions. However, the basic problem in applying a single-particle state atomic (bosons) equation to the aggregate of tumor cells is that while the atoms are quantum particles and their wave functions may be represented by a complex function, the biological cells are classical objects and must be represented by real functions. Here we describe how the Gross-Pitaevskii (GP) equation (a mean-field approximation version of the complex single-particle state Heisenberg equation) could be regarded as a coupling of two real classical wave equations and employed to model the morphology and growth dynamics of benign tumors successfully.

In vitro simulations of benign tumors in three dimensions have revealed that they are finite-size and inhomogeneous aggregates of cancer cells, which appear in a bound spheroid form [4–6]. In vitro tumor culture data [4] reveals a strong oscillatory pattern for the proliferating cell count with intricate features of partial collapse and regrowth. Although the collapse may be attributed to the start of a necrotic process [4], there is no current explanation, either from mathematical models or biological data, to explain the subsequent spurt in growth, since in an in vitro growth angiogenesis or neo-vascularization [7] are not possible and the necrotic waste, which is a toxic product, is unlikely to trigger a spurt in growth. During avascular growth (benign tumor) or its in vitro simulation, the diffusion of nutrients attenuates in the central region as the tumor grows in size. Consequently, the cells in the central region grow slowly and some enter a quiescent phase, where they no longer proliferate. With further increase in tumor size, where nutrient diffusion into the central region is further reduced, some of the quiescent cells enter a necrotic phase and the tumors develop a central necrotic core [4]. As the necrotic contribution increases, the avascular tumors enter a dormant phase, striking a balance between the rates of mitosis and necrosis. Experimentally, it has been found that before entering the dormant phase, the cell count shows a great deal of fluctuations [4] mentioned above. This strong fluctuation, which has been described in [2, 3], may result from squeezing and relaxation of the tumor during its oscillations, and has never been addressed by any other theoretical model.

In previous theoretical modeling of tumors, the emphasis was given to the simulation of tumor morphology, immune response and estimation of the effect of administered drugs [8–16]. The simplest tumor model uses ordinary first-order differential equations in an empirical form and simulates cell number or volume growth by using various mitosis and necrosis rates and immunological reactions [8, 9]. Such models do not consider any of the physical interactions occurring in the cell aggregate. The second type of study employs spatio-temporal (diffusion-type) equations [10–12], which include cell mobility or kinetic factors, or use a cellular automaton model [13–15] to simulate the tumor structure by minimizing the energy of the system with each additional cell added to the aggregate. These calculations explicitly consider cell-cell interactions, and show that these interactions play a crucial role in determining the dormant size (for benign tumors), the morphology and the growth dynamics of a tumor [13–15]. However, these results do not reproduce the oscillatory nature of the in vitro proliferation dynamics. This points towards the presence of non-linear potentials in the cell aggregate and the necessity of treating the tumor as a *bound state* of cancer cells. As far as the non-linear effects are concerned, their effects have been studied elaborately in connection with immunological reactions in the growth profile of a tumor [16]. Apart from the non-linear cell-cell interaction, the behavior of the tumor's growth might be severely affected by the influence of the surrounding medium. In the non-linear matter wave model [2, 3] described below, both the non-linear cell-cell interactions and the effect of the external field is taken into account considering that the aggregate of cells in the tumor is in an energy minimized bound state arising out of their kinetic energy, interaction potential energy, and the potential energy from the external field of the surrounding medium and water.

Methodology

Single-particle state Gross-Pitaevskii (GP) equation and its dimensionless form

The time-evolution dynamics of a single-particle state bosonic condensate with feeding of atoms to the condensate from the thermal cloud and loss of atoms from the condensate through recombinations is described by the extended GP equation [17, 18]:

$$i\mathrm{h}\frac{\partial}{\partial t}\Phi = \left[-\frac{\mathrm{h}^2}{2m}\nabla^2 + \frac{4\pi\mathrm{h}^2 a}{m}|\Phi|^2 + V_{ext} + i\frac{\gamma}{2}\mathrm{h}\omega - 2i\xi\left(\frac{4\pi\mathrm{h}a}{m\omega}\right)^2 \mathrm{h}\omega|\Phi|^4\right]\Phi \tag{1}$$

where the two-body atom-atom interaction is described by the s-wave scattering length a and is represented as: $v(r, r') = 4\pi h^2 a/m \times \delta(r - r')$; where m is the mass of the atoms; δ is the Dirac delta function. For two-body attractive interactions, a is negative in sign, while for repulsive interactions the sign of a is positive. γ and ξ are parameters

concerning feeding to and dissipation from the condensate. The term proportional to γ provides an exponential growth for the order parameter Φ and hence for the number density $|\Phi|^2$. The $|\Phi|^4$ term leads to a clustering of two atoms into a dimer formation from three-body interactions. This results in a loss of atoms from the condensate wave function Φ in the form of dimer.

$$N(t) = \int |\Phi(r,t)|^2 d^3r \tag{2}$$

$$\langle R^2(t)\rangle = \frac{\int r^2|\Phi(r,t)|^2 d^3r}{\int |\Phi(r,t)|^2 d^3r} \tag{3}$$

Dividing Eq. (1) by $\hbar\omega$ and introducing a dimensionless length: $x = \left(\sqrt{2}/l_0\right)r$ (where $l_0 = \sqrt{\hbar/m\omega}$), and time: $\tau = \omega t$, we recast Eq. (1) as

$$i\hbar\frac{\partial}{\partial\tau}\Phi = \left[-\nabla_x^2 + \eta|\Phi|^2 + \mathcal{V}(x) + i\frac{\gamma}{2} - 2i\xi\eta^2|\Phi|^4\right]\Phi \tag{4}$$

Here $V(x) = V_{ext}/\hbar\omega$ *and* $\eta = 4\pi a l_0^2$. Using a dimensionless order parameter: $\phi(x,\tau) = \sqrt{4\pi|a|l_0}\Phi$ we arrive at the following complex wave equation [2, 3]:

$$i\frac{\partial}{\partial\tau}\phi(x,\tau) = \left[-\nabla_x^2 - |\phi|^2 + V(x) + i\gamma' - i\xi'|\phi|^4\right]\phi(x,\tau) \tag{5}$$

where ϕ is a complex matter field representing the atoms in the condensate; $\gamma' = \gamma/2$, $\xi' = 2\xi$, and the negative sign of the scattering length a (attractive interaction) is explicitly taken into account in Eq. (5).

Equivalence of GP equation with two coupled equations with real components

For application of the GP equation to a classical system we interpret ϕ as a two component field with real components ϕ_1 and ϕ_2 where $\phi = \phi_1 + i\phi_2$. In terms of these real components, one can rewrite Eq. (5) in the form of two coupled equations as follows:

$$\begin{aligned}\frac{d}{d\tau}\phi_1(x,\tau) =& -\nabla_x^2\phi_2(x,\tau) - |\phi|^2\phi_2(x,\tau)\\ &+ V(x)\phi_2(x,\tau) + \gamma'\phi_1(x,\tau)\\ &- \xi'|\phi|^4\phi_1(x,\tau)\end{aligned} \tag{6}$$

$$\begin{aligned}\frac{d}{d\tau}\phi_2(x,\tau) =& \nabla_x^2\phi_1(x,\tau) + |\phi|^2\phi_1(x,\tau) - V(x)\phi_1(x,\tau)\\ &+ \gamma'\phi_2(x,\tau) - \xi'|\phi|^4\phi_2(x,\tau)\end{aligned} \tag{7}$$

Rearranging, we rewrite them as:

$$\begin{aligned}\frac{d}{d\tau}\phi_1(x,\tau) =& \gamma'\phi_1(x,\tau) - \xi'|\phi|^4\phi_1(x,\tau)\\ &- \left[\nabla_x^2 - V(x) + |\phi|^2\right]\phi_2(x,\tau)\end{aligned} \tag{8}$$

$$\begin{aligned}\frac{d}{d\tau}\phi_2(x,\tau) =& \gamma'\phi_2(x,\tau) - \xi'|\phi|^4\phi_2(x,\tau)\\ &+ \left[\nabla_x^2 - V(x) + |\phi|^2\right]\phi_1(x,\tau)\end{aligned} \tag{9}$$

From Eqs. (8) and (9), we see that the first term of the right hand side (r.h.s) can give rise to the so-called first-generation tumor model, providing exponential growth with the growth rate determined by the parameter γ'. The second term on the r.h.s accounts for depletion in the cell number that resembles necrosis and in this model this necrotic contribution is taken as proportional to the square of number density ρ (where $\rho = |\phi|^2$ in dimensionless units mentioned above); the proportionality constant being the parameter ξ'. The rest are coupling terms concerning diffusion, external potential, and cell-cell interaction, respectively. The model, as it stands now, introduces a simplification in terms of having the same growth and depletion rates for both ϕ_1 and ϕ_2 components. This simplification allows us to combine the two equations into a complex field equation (Eq. 5), which is solved numerically. For simplicity of the numerical task, we restrict the application to in vitro growth of multicellular tumors in three dimensions, which reveal a spherical symmetry [4]. Assuming the external potential $V(x)$ to be spherically symmetric, as is the case for an in vitro tumor growth, and defining $\varphi = \varphi \times x$, we arrive at the following equation in one dimension:

$$i\frac{\partial}{\partial\tau}\varphi(x,\tau) = \left[-\frac{d}{dx^2} - \frac{|\varphi|^2}{x} + V(x) + i\gamma' - i\xi'\frac{|\varphi|^4}{x^4}\right]\varphi(x,\tau) \tag{10}$$

In terms of φ, the number of particles in the bound state and the mean-square radius of the bound state are given by:

$$\begin{aligned} N(t) &= \int |\Phi(r,t)|^2 d^3r \\ &= \frac{4\pi}{8\pi|a|}\frac{l_0}{\sqrt{2}} \times \int |\varphi(x,\tau)|^2 dx \\ &= \frac{1}{2\sqrt{2}|a|} l_0 \times n(\tau) \end{aligned} \tag{11}$$

$$\begin{aligned} \langle R^2(t)\rangle &= \frac{\int r^2 |\Phi(r,t)|^2 d^3r}{\int |\Phi(r,t)|^2 d^3r} \\ &= \frac{l_0^2}{2} \times \frac{\int x^2 |\varphi(x,\tau)|^2 dx}{\int |\varphi(x,\tau)|^2 dx} = \frac{l_0^2}{2}\langle x^2(\tau)\rangle \end{aligned} \tag{12}$$

where $n(\tau) = \int |\varphi(x,\tau)|^2 dx$.

Length scaling of the coupled matter wave equation

To simulate the tumor, we study a trial value of l_0 of the form: [2, 3, 19]

$$L_0 = \mathrm{l}_0 \times \frac{\text{effective size of cell in tumor}}{\text{effective size of atom in condensate}} \tag{13}$$

Similar correlations between classical statistical mechanics and multicellular systems have been studied previously by Arlotti et al. [20] The length scaling redefines the cell number and the tumor radius as:

$$\begin{aligned} N(\tau) &= \frac{1}{2\sqrt{2}|a|} L_0 \times n(\tau) \\ &= \left(\frac{\mathrm{l}_0}{\sqrt{2d}}\right) \times \left(\frac{D}{2|a|}\right) \times n(\tau) : \left(\frac{\mathrm{l}_0}{\sqrt{2d}}\right) \times n(\tau) \end{aligned} \tag{14}$$

$$R(\tau) = \frac{L_0}{\sqrt{2}}\sqrt{\langle x^2(\tau)\rangle} = \left(\frac{\mathrm{l}_0}{\sqrt{2d}}\right) \times D \times \sqrt{\langle x^2(\tau)\rangle} \tag{15}$$

The value of D, the effective size of a cell, is obtained from the measured data of [4] while the value of l_0/d is fixed by selecting an appropriate solution of the GP Eq. (5) for the short-range, attractively interacting, and externally trapped atomic condensate [17, 18].

Time-independent form of the coupled matter wave equation

Considering $V(x) = V_{ext}/h\omega$ we write down the stationary form of Eq. (10) as:

$$\left[-\frac{d}{dx^2} - \frac{|\psi|}{x} + V(x)\right]\psi = \beta\psi \tag{16}$$

where $\beta = \mu/\omega$; μ representing the chemical potential (average single-particle energy). This Eq. (16) has various stable, metastable, or unstable solutions [21] correspond-

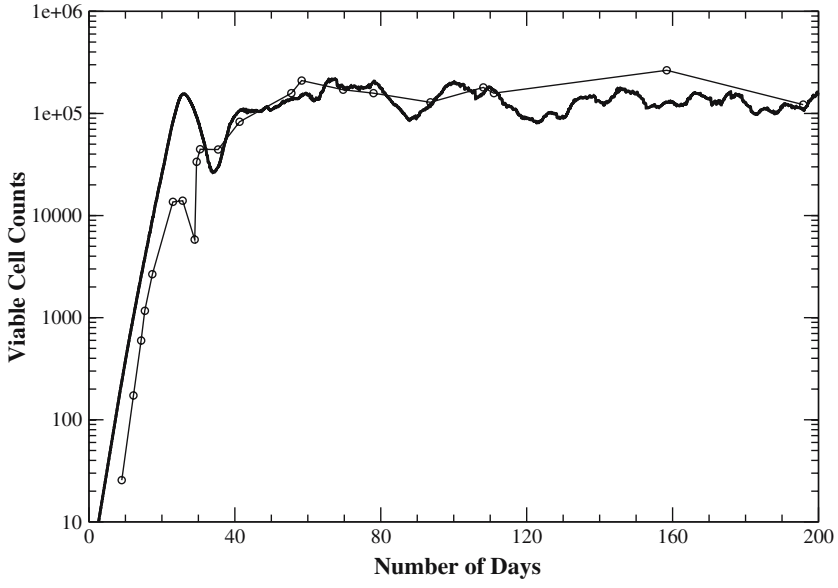

Fig. 1 In vitro growth profile of a benign tumor. Culture data of Folkman and Hochberg [4] for the multicellular spheroids developed in agar with V79 Chinese hamster lung cells (*circles*); simulation results as obtained from the coupled non linear matter wave equations (*thick solid line*)

ing to various values of β. Each solution corresponds to a particular value of $N|a|/l_0$ (see Eq. 11).

Numerical methods

The time-independent Eq. (16) is solved numerically using the Runge-Kutta method [22] as described in the work of Edward and Burnett [23], and Gammal et al. [24] and employed in previous calculations [2, 3]. This equation has various solutions depending on the number of particles [21, 24]. We choose a minimum-energy solution with only a few particles and then propagate the solution in time by feeding it to Eq. (5). The time-dependent Eq. (5) is discretized using the Crank-Nicholson difference [22] and the resulting set of tri-diagonal equations are solved using the Gaussian elimination method [22] as implemented in [2, 3].

Results and discussions

In this work, we focus on the simulation of the experimental data for the growth of multicellular spheroids that developed when V79 Chinese hamster lung cells are

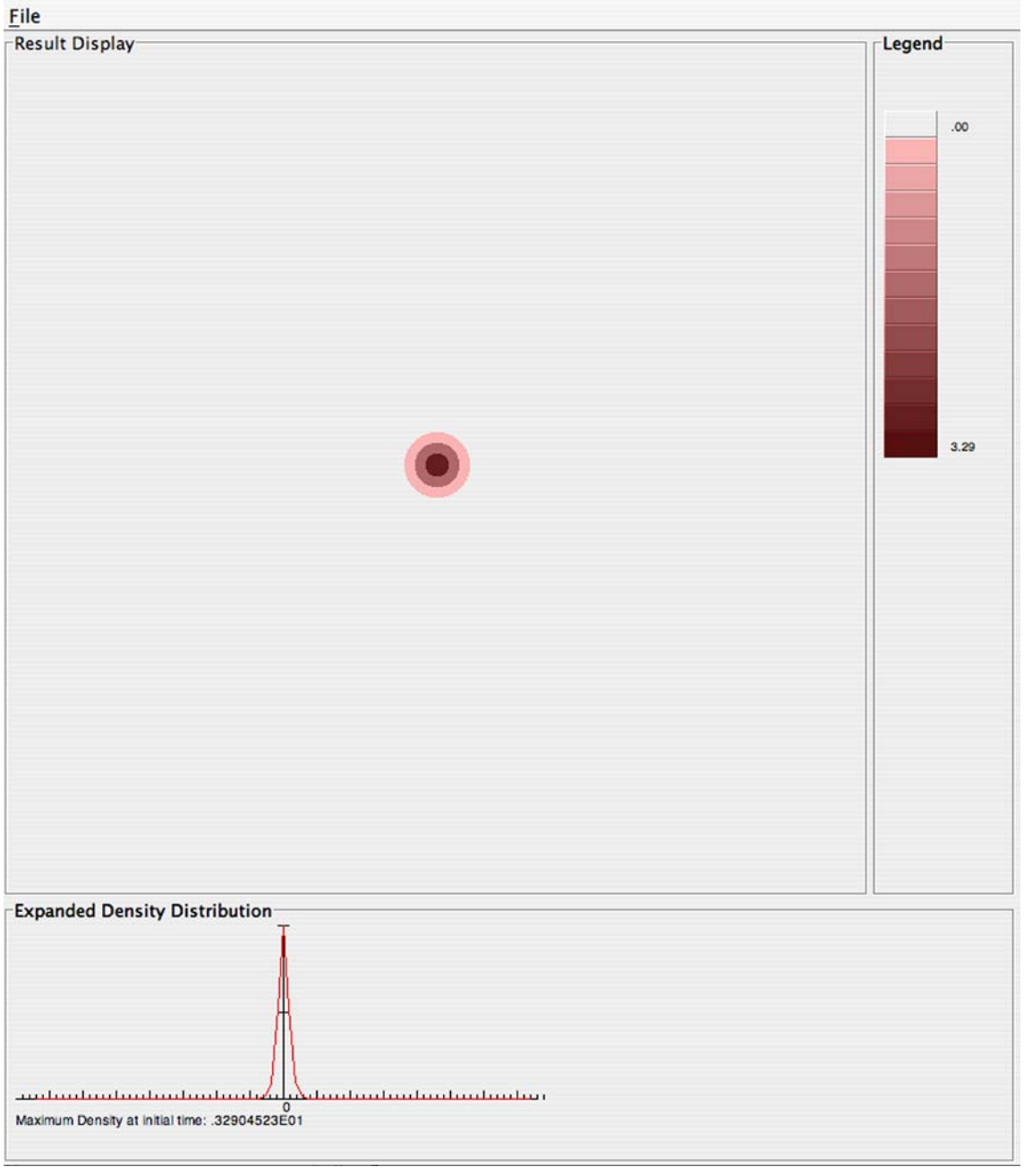

Fig. 2 Screen shot from the graphical analysis tool showing clustering of cells in the initial tumor (*up*); cell density profile (*down*)

grown in soft-agar. We approximate the hydration effect of agar on the cell aggregate as a constant gauge potential experienced by the cells. We model it by $V(x) = V_0$. Firstly, we solve the time-independent form of the single-particle state Gross-Pitaevskii Eq. (16) for different bound-state solutions as a function of various sets of values for V_0 and β (the constant gauge potential can be absorbed in the redefinition of β). Despite the constant external gauge potential, the stationary solution is stable due to the attractive nature of the cell-cell interactions. Then, we propagate each solution in time, employing Eq. (5) and plot the number of cells (as obtained from Eq. 14) against time. In Fig. 1, the experimental result for the V79 cell colony and the theoretical results for the proliferating cell count obtained with V_0=1.5, γ=0.5, and ξ=0.001 are shown. It can be seen that there is significant agreement between the two

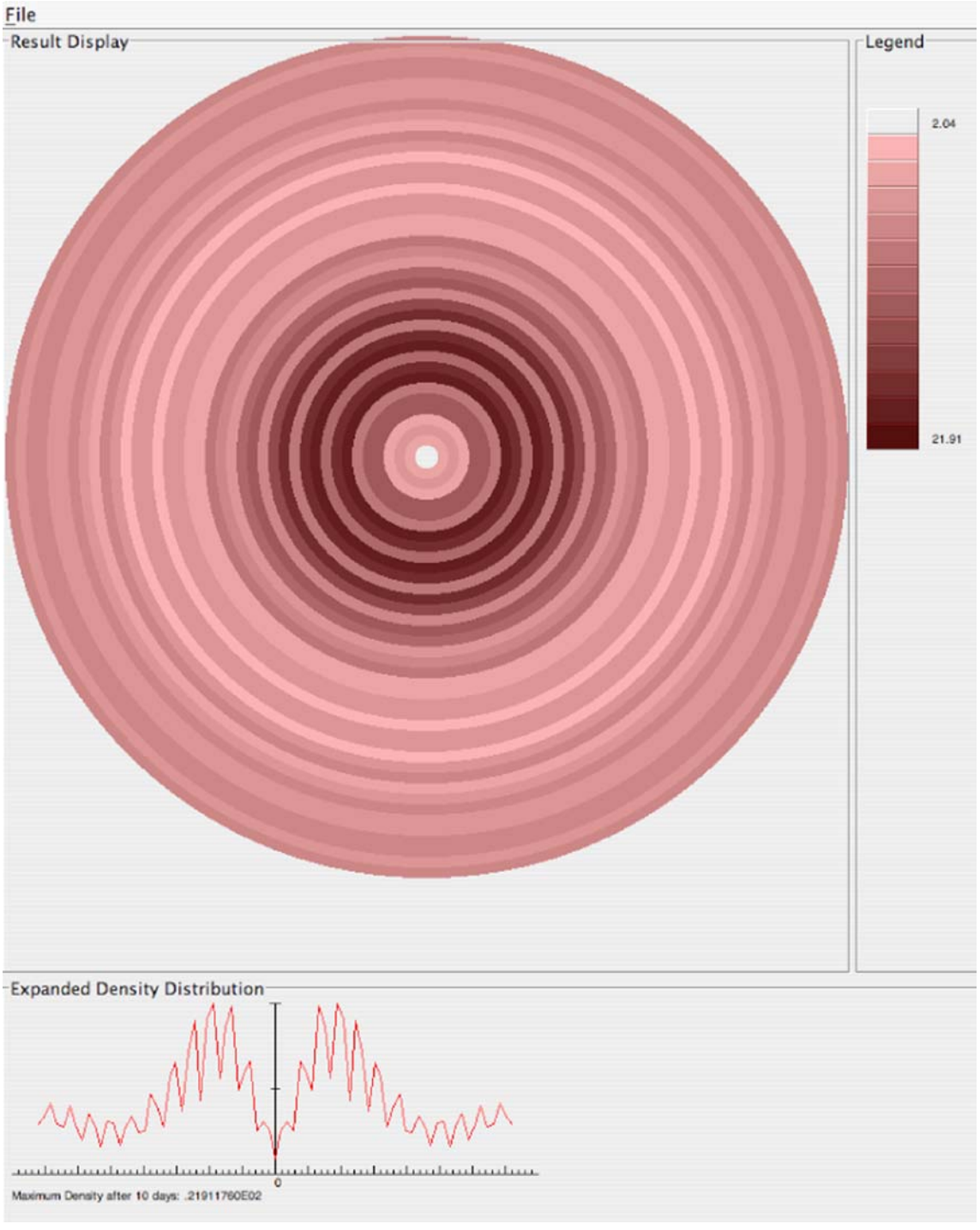

Fig. 3 Screen shot from the graphical analysis tool showing simulation results after 10 days: clustering of cells of the tumor (*up*); cell density profile (*down*)

sets of results once the time scale ($t = \tau/\omega$) is chosen such that ω corresponds to a value ω~1 per day, that is $\omega = 1/(24 \times 60 \times 60)$ sec ^{1}.

From the measured proliferation count (solid curve with circles; Fig. 1), we find that 1) initially the number of cells increases in a steep exponential fashion; 2) it attains a local peak at around day-23; 3) next it suffers a partial collapse; 4) after completing the collapse, it again starts a strong exponential growth at around day-29. The second experimental growth phase had a short duration and gradually stabilizes with a viable cell count around N~10^5. From the thick solid curve of Fig. 1, we see that all the characteristic features of tumor growth described above are present in the theoretical results, including the approximate positions of the peaks, collapse, and re-growth.

To understand the collapse and re-growth phenomena described above, we study the density profile of the cell aggregate. We find that as the cell number increases, the central density (in units of $|\varphi(x,t)/x|^2$) also increases rapidly, leading to a greater contribution to the necrotic process. When the central density reaches a maximum of 10^4 near day-24, the increased attractive potential triggers a visible partial collapse of the cell aggregate; with the central region being affected the most. In the process of collapse, there appears an increase in the clustering of cells and consequent necrotic contribution leading to the formation of a necrotic core [4, 13]. The contribution to the necrotic core diminishes the attractive potential in tumor (in its bound state), which results in a volume expansion of the tumor. As the volume expands, the cell-density decreases, which in turn paves the way for a greater nutrient diffusion. A greater nutrient diffusion might be responsible for the second exponential growth, which according to the model is possible because of an oscillation of tumor volume. While the model explicitly reveals the oscillation in tumor size, the impetus in the growth arises in part from a sharp decrease in the necrotic contribution and also in part from the diffusion term (although, the diffusion term here represents cell diffusion).

To achieve a more critical understanding of the cell proliferation kinetics, we have developed a graphical analysis tool to study the tumor growth. Figure 2 represents the initial tumor as given by the solution of the time-independent Eq. (16). From the plot of the density distribution of the cells we find that initially the cell growth and proliferation occur mostly at the center, leading the cell density to be the highest at the center. This eventually leads to necrosis in this central region, as the higher cell density retards the nutrient diffusion. In this model, the above scenario has been captured by introducing a term in the equation that provides attenuation of proliferating cells as a function of $(density)^2$. From Fig. 3, we see that this term leads to the modeling of a central necrotic core. Also from the diagram, we find that the central necrotic core is surrounded by densely proliferating cells and the cell density resembles an onion-type structure. The graphical analysis enables us to visualize and understand the density profile of the proliferating cells, which is crucial information in order to optimize the effect of drugs. Our current work is addressing this latter issue.

Summary and conclusions

We present here an application of the non-linear Schrödinger equation to the cell aggregate of a multicellular tumor considering it as a coupling of two wave equations with real components. The simulation results reproduce the experimentally observed oscillatory pattern in the growth profile of a tumor and explain the spurt in cell growth in the aftermath of a partial collapse in terms of a volume expansion and resulting increment in the nutrient diffusion due to a lesser attractive potential of the cell aggregate. The study indicates that the necrotic contribution during the growth of a tumor could be preceded by a small localized clustering of cells, thus reducing the probability of nutrient diffusion inside the cluster. The graphical analysis described here provided us with invaluable information about the time evolution of the density profile of the proliferating cells, which is essential in developing effective strategies for administering drugs.

Acknowledgements Authors thank Drs. Crystal Weyman and Joseph Fontes for reading the manuscript and providing their valuable suggestions. We acknowledge the financial support from the Department of Energy (grant number: DE FG02 03ER15462). TF acknowledges the partial financial support from FAPESP and CNPq of Brazil.

References

1. Lodish H, Berk A, Matsudaira P, Kaiser CA, Krieger M, Scott MP, Lawrence Zipursky S, Darnell J (2004) Molecular Cell Biology, 5th edn. Freeman WH and Company, New York, p 941
2. Biswas PK, Pacheco MTT (2005) Math comp modeling 41:1299 1306
3. Biswas PK, Germano JSE (2004) Int J Nonl Sc Numerical Siml 5:149 156
4. Folkman J, Hochberg M (1973) J Expt Medicine 138:745 753
5. Sutherland RM, McCredie JA, Inch WR (1971) J Natl Cancer Inst 46:113 120
6. Dalen H, Burki HJ (1971) Exp Cell Res 65:433 438
7. Folkman J (1971) New England J of Medicine 285:1182 1186
8. Miklavcic D, Jarm T, Karba R, Sersa G (1995) Math Comp Simulation 39:597 602 and references therein
9. Kuznetsov VA, Knott GD (2001) Math Comp Modeling 33:1275 1287 and references therein
10. Tracqui P, Cruywagen GC, Woodward DE, Bartoo GT, Murray JD, Alvord EC Jr (1995) Cell Prolif 28:17 31
11. Burgess PK, Kulesa PM, Murray JD, Alvord EC Jr (1997) J Neuropath Expt Neur 56:704 713
12. Maggelakis SA, Adam JA (1990) Math Comp Model 13:23 38
13. Stott EL, Britton NF, Glazier JA, Zajac M (1999) Math Comp Modeling 30:183 198
14. Dormann S, Deutsch A (2002) In Silico Biology 2:393 406
15. Mombach JCM (1993) Phys Rev E 48:598 602
16. Bellomo N, Firmani B, Guerri L (1999) Appl Math Letters 12:39 44

17. Kagan Yu, Muryshev AE, Shlyapnikov GV (1998) Phys Rev Lett 81:933 937
18. Filho VS, Gammal A, Frederico T, Tomio L (2000) Phys Rev A 62:033605/1 033605/4
19. Biswas PK, Pacheco MTT (2003) Los Alamos National Laboratory, Preprint Archive, Condensed Matter. 1 13, arXiv: cond mat/0306539
20. Arlotti L, Bellomo N, de Angelis E (2002) Math Models Meth Appl Sci 12:567 591
21. Gammal A, Frederico T, Tomio L, Chomaz Ph (2000) J Phys B 33:4053 4067
22. Press WH, Flannery BP, Teukolsky SA, Vetterling WT (1996) Numerical recipes in fortran 77 the art of scientific comput ing, 2nd edn. Cambridge University Press, p 42, pp 840 844
23. Edwards M, Burnett K (1995) Phys Rev A 51:1382 1386
24. Gammal A, Frederico T, Tomio L (1999) Phys Rev E 60:2421 2424